Advanced Modeling of Cyclotron Wave Heating and Current Drive in Toroidal Plasmas Based on Integro-Differential Full Wave Analysis

A. Fukuyama 1), S. Murakami 1), T. Yamamoto 1), and H. Nuga 1)

1) Graduate School of Engineering, Kyoto University, Kyoto, Japan

e-mail contact of main author: fukuyamanucleng.kyoto-u.ac.jp

Abstract. Self-consistent and accurate modeling of wave-plasma interactions is one of the key issues in producing and sustaining burning plasmas. We have upgraded our full wave component of the integrated modeling code TASK, taking account of the finite gyroradius effects indispensable for correctly describing the absorption of ICRF waves by energetic ions and the behavior of electron Bernstein waves. The integro-differential full wave analysis was coupled with the Fokker-Planck analysis and the GNET code to describe the modification of the momentum distribution function and to calculate the power deposition profile including the finite orbit size effects. These advanced modeling provides more accurate evaluation of the efficiency of wave heating and current drive in tokamaks and helical configurations. The newly-updated TASK/WM component is first applied to the analysis of the electron Bernstein waves in a small-size spherical tokamak plasmas and the driven current is evaluated from the Fokker-Planck analysis. Next the power absorption by alpha particles during the ICRF heating in tokamak plasmas is evaluated with the finite gyroradius effect taken into account. Finally the power deposition profile during the ICRF heating in the three-dimensional LHD configuration is calculated by taking account of the finite gyroorbit effect.

1. Introduction

Self-consistent and accurate modeling of wave-plasma interactions is one of the key issues in producing and sustaining burning plasmas. We have upgraded our full wave component of the integrated modeling code TASK [1], taking account of the finite gyroradius effects indispensable for correctly describing the absorption of ICRF waves by energetic ions and the behavior of electron Bernstein waves. The integro-differential full wave analysis was coupled with the Fokker-Planck analysis and the GNET code [2] to describe the modification of the momentum distribution function and to calculate the power deposition profile including the finite orbit size effects. These advanced modeling provides more accurate evaluation of the efficiency of wave heating and current drive in tokamaks and helical configurations.

2. Integro-differential full wave analysis

The finite gyroradius effects are essential in the wave-particle interaction with short-wavelength waves ($k_\perp \rho \gtrsim 1$) or near the cyclotron harmonics ($\omega \simeq \ell \omega_c$) where $k_\perp$ is the perpendicular wave number, ρ is the gyroradius, ω is the wave frequency, and ω_c is the cyclotron frequency. The analysis with differential operators is usually limited up to the second order harmonics and not applicable for $k_\perp \rho \gtrsim 1$. The approach in three-dimensional Fourier space requires very large computation resources. We have formulated the integral representation of the dielectric tensor $\overleftrightarrow{\epsilon}$ and employed it in the boundary problem of Maxwell's equation for the wave electric field

$$\boldsymbol{E} = \boldsymbol{E}(\boldsymbol{r})\,\mathrm{e}^{-\mathrm{i}\omega t} = \sum_{mn} \boldsymbol{E}^{mn}(s)\,\mathrm{e}^{\mathrm{i}m\chi+\mathrm{i}n\zeta-\mathrm{i}\omega t}$$

$$\nabla\times\nabla\times\boldsymbol{E}(\boldsymbol{r}) + \frac{\omega^2}{c^2}\int \overleftrightarrow{\epsilon}(\boldsymbol{r},\boldsymbol{r}')\cdot\boldsymbol{E}(\boldsymbol{r}')\mathrm{d}\boldsymbol{r}' = \mu_0\boldsymbol{J}_{ext}(\boldsymbol{r}') \tag{1}$$

$$\overleftrightarrow{\epsilon}^{m'n'mn}(s,s') = \frac{\omega_\mathrm{p}^2}{\omega}\sum_\ell \int \mathrm{d}s_0 \int_0^{2\pi}\mathrm{d}\chi_0 \int_0^{2\pi}\mathrm{d}\zeta_0\,\mathrm{e}^{\mathrm{i}\{(m'-m)\chi_0+(n'-n)\zeta_0\}}\overleftrightarrow{K}_\ell(s,s',s_0,\chi_0,\zeta_0) \tag{2}$$

where s denotes the radial variable of the flux coordinates and s_0, χ_0 and ζ_0 represent the radial, poloidal and toroidal coordinates of the guiding center position, respectively. The integer ℓ is the cyclotron harmonic number. The wave electric field is Fourier-decomposed with the poloidal mode number m and the toroidal mode number n and the finite element method is used in the radial direction. We have obtained an explicit expression of the kernel function K for a plasma with the Maxwellian distribution, which is localized in the region $|s-s_0| \lesssim 3\rho$ and $|s'-s_0| \lesssim 3\rho$. This new version of the full wave component TASK/WM will be available for two-dimensional tokamak configuration and three-dimensional helical configuration shortly.

3. Electron Bernstein waves in ST plasmas

In a spherical tokamak (ST) configuration, central heating by ECRF waves is prevented by cut-off layers due to high density and cyclotron harmonics layers due to low aspect ratio. In order to describe the penetration over the cutoff layer, full wave analysis including the electron Bernstein wave (EBW) is necessary. We have employed TASK/WM to describe the extraordinary wave in a small-size ST configuration as shown FIG. 1. The propagation and absorption change according to the location of the plasma cutoff density. In a high temperature plasma, the electromagnetic wave is mode-converted to the EBW. Full wave analysis of the mode conversion and the cyclotron harmonics damping in a simple configuration as well as the small ST configuration are presented. With the Fokker-Planck analysis, the current drive efficiency by the EBW will be evaluated.

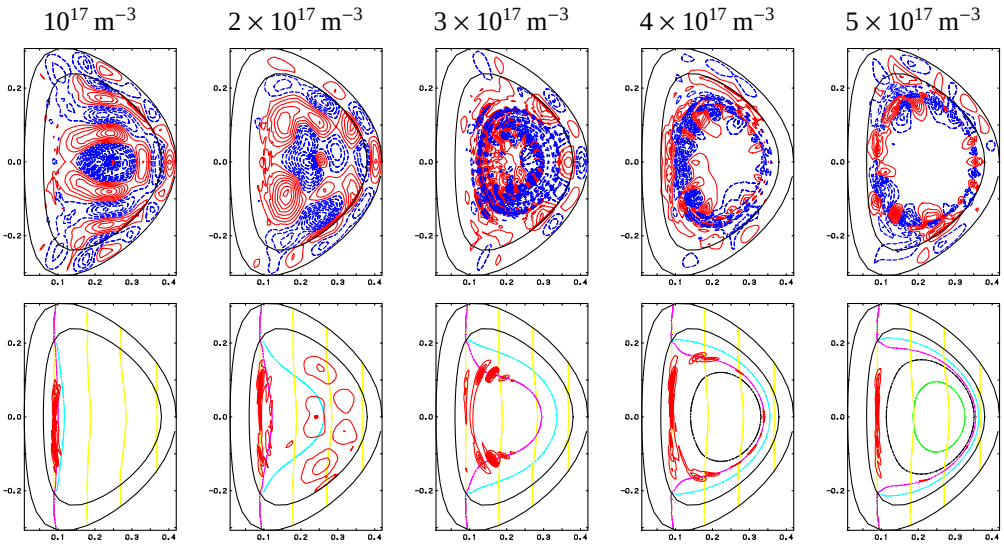

FIG. 1. Density dependence of electron cyclotron wave propagation and absorption. Upper and lower figures indicate contours of the poloidal wave electric field and the electron power absorption, respectively. The power deposition localizes near the upper hybrid resonance layer except the case of highest density.

4. Absorption by energetic ions in ICRF heating

The absorption of ICRF waves by energetic ions is sensitive to the finite gyroradius effects. The TASK code was applied to evaluate the absorption by energetic ions produced by neutral beam injection and fusion reaction. The time evolution of the high energy tail in the ion momentum distribution $f(p)$ was self-consistently calculated by the Fokker-Planck component TASK/FP. The distribution $f(p)$ is approximated by a sum of Maxwellian distributions with different anisotropic temperatures in the integro-differential approach to the full wave analysis. The result is compared with that of the differential approach applicable to arbitrary momentum distribution function.

5. Evaluation of heating efficiency

In order to clarify the finite orbit effect of energetic ions, the current drive efficiency, and the toroidal flow generation, we carried out global simulation study which takes into account the wave-plasma interaction self-consistently.

5.1. Simulation model

In this study we combine two simulation code to study the ICRF heating. First, Maxwell's equation for RF wave is solved by TASK/WM code, then the obtained RF wave electric field profile is used to solve a drift kinetic equation by GNET code. Finally, the steady state velocity distribution function of plasma is obtained.

GNET code solves a linearized drift kinetic equation for energetic ions including complicated behavior of trapped particles in 5-D phase space as

$$\frac{\partial f}{\partial t} + (\boldsymbol{v}_{\parallel} + \boldsymbol{v}_{\mathrm{D}}) \cdot \nabla f + \boldsymbol{a} \cdot \nabla_{\boldsymbol{v}} f - C(f) - Q_{\mathrm{ICRF}}(f) - L_{\mathrm{particle}} = S_{\mathrm{particle}}, \tag{3}$$

where $C(f)$ and Q_{ICRF} are the linear Coulomb collision operator and the ICRF heating term, respectively. S_{particle} and L_{particle} are the particle source term by ionization of neutral particles and sink (loss) term including orbit loss and charge exchange, respectively.

In order to solve the linearized drift kinetic equation (3) by Monte Carlo method, the Green function, $\mathcal{G}$, is introduced as

$$\frac{\partial \mathcal{G}}{\partial t} + (\boldsymbol{v}_{\parallel} + \boldsymbol{v}_{\mathrm{D}}) \cdot \nabla \mathcal{G} + \boldsymbol{a} \cdot \nabla_{\boldsymbol{v}} \mathcal{G} - C(\mathcal{G}) - Q_{\mathrm{ICRF}}(\mathcal{G}) - L_{\mathrm{particle}} = 0 \tag{4}$$

with the initial condition $\mathcal{G}(\boldsymbol{x}, \boldsymbol{v}, t = 0 | \boldsymbol{x}', \boldsymbol{v}') = \delta(\boldsymbol{x} - \boldsymbol{x}')\delta(\boldsymbol{v} - \boldsymbol{v}')$. The $\mathcal{G}$ is evaluated by solving the equation of motion for guiding center of test particles expressed by the Hamiltonian of charged particle

$$H = \frac{1}{2} m v_{\parallel}^2 + \mu B(\psi, \theta, \varphi) + q\Phi(\psi) \tag{5}$$

in Boozer coordinate. In order to solve the equation of motion, 6th-order Runge-Kutta method is applied. The collisional effects are taken into account using the linear Monte Carlo collision operator [4].

The ICRF heating term is modelled by changing the perpendicular velocity of the test particle passing through the resonance layer, $\omega - k_{\parallel} v_{\parallel} = n\Omega$, by

$$\begin{aligned}\Delta v_{\perp} \approx & \left[\left(v_{\perp 0} + \frac{q}{2m} I|E_+| J_{n-1}(k_{\perp}\rho)\cos\phi_{\mathrm{r}}\right)^2 + \frac{q^2}{4m^2}\left\{I|E_+| J_{n-1}(k_{\perp}\rho)\right\}^2 \sin^2\phi_{\mathrm{r}}\right]^{-\frac{1}{2}} \\ & - v_{\perp 0} \approx \frac{q}{2m} I|E_+| J_{n-1}(k_{\perp}\rho)\cos\phi_{\mathrm{r}} + \frac{q^2}{8m^2 v_{\perp 0}}\left\{I|E_+| J_{n-1}(k_{\perp}\rho)\right\}^2 \sin^2\phi_{\mathrm{r}}, \end{aligned} \tag{6}$$

where E_+ and ϕ_{r} are the left-circularly polarized component of RF wave electric field and random phase, respectively. Also, q, m, ρ, J_n are the charge, mass, the Larmor radius of the particle and nth Bessel function, respectively. The time duration passing through the resonance layer, I, is given by the minimum value as, $I = \min(\sqrt{2\pi/n\dot{\Omega}}, 2\pi(n\ddot{\Omega})^{-1/3}\mathrm{Ai}(0))$, which corresponds to two cases; the simple passing of the resonance layer and the passing near the turning point of a trapped motion (banana tip).

In the simulation $|E_+|$ evaluated by TASK/WM is used in Eq. (6). We consider only fundamental ion cyclotron resonance and assume $k_{\perp}\rho$ is small in this study. Therefore,

$$|E_+| J_{n-1}(k_{\perp}\rho) \approx |E_+|. \tag{7}$$

Assuming $B_{\varphi} \gg B_{\theta}$, $k_{\parallel}$ is evaluated as

$$k_{\parallel} \approx \frac{n}{R}, \tag{8}$$

where n is the toroidal mode number in Eq. (**??**) and R is the major radius.

Finally the velocity distribution function is calculated by integrating the particle in the phase space over initial position $(\boldsymbol{x}', \boldsymbol{v}')$ and initial time t' as

$$f(\boldsymbol{x}, \boldsymbol{v}, t) = \int_0^t dt' \int d\boldsymbol{x}' \int d\boldsymbol{v}' S_{\text{particle}}\, \mathcal{G}(\boldsymbol{x}, \boldsymbol{v}, t - t' | \boldsymbol{x}', \boldsymbol{v}'). \tag{9}$$

5.2. Simulation results

We study the ICRF minority heating applying the developed code in the simple tokamak plasma. The cross section of the MHD equilibrium by VMEC code are shown in Fig. 2. The plasma parameters are listed in Table . We assume deuterium (D) as a majority ion and hydrogen (H) as a minority ion.

We first analyze the ICRF wave propagation and absorption in the plasma by TASK/WM. Fig. 3 (a) and (b) are contour plots of the real part of left circularly polarized component of the RF electric field, $\mathrm{Re}\, E_+$ (left) and the power absorption (right) on the poloidal cross section in the case of the ICRF wave frequency $f_{\mathrm{RF}} = 42\,\mathrm{MHz}$ (on axis heating). Fig. 3 (c) and (d) are the same manner in the case of $f_{\mathrm{RF}} = 45\,\mathrm{MHz}$ (off axis heating). The ICRF waves are exited in the plasma from the antenna set on the outer side of the torus (right side). In the both cases, the $\mathrm{Re}\, E_+$ component of the waves are absorbed and the wave amplitude is damped at the minority ion cyclotron resonance layer (green lines in the left figure of Fig. 3. Then the amplitude is damped further near the two-ion-hybrid cutoff and resonance layers.

TABLE I: Paarameters of tokamak plasma

Plasma major radius	R_0	3.6 m
Plasma minor radius	a	0.6 m
Magnetic field at magnetic axis	B_0	3.0T
Temperature at magnetic axis	T_0	3.0keV
Temperature on plasma boundary	T_s	0.3keV
Density at magnetic axis	n_0	$1.0\times10^{20}/\mathrm{m}^3$
Density on plasma boundary	n_s	$0.1\times10^{20}/\mathrm{m}^3$
Antenna current density	j_{ext}	1.0A/m
Wave frequency	f_{RF}	42, 45MHz
Minority ion ratio	H/D	5%
Collisionality	ν_s	0.003

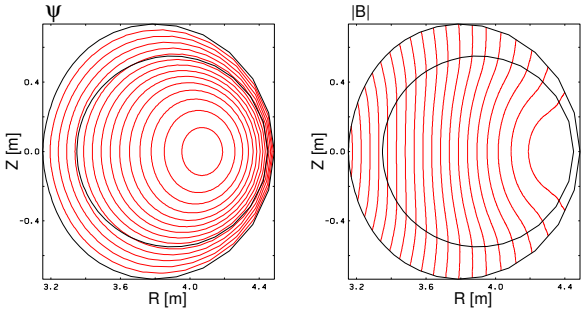

FIG. 2. Equilibrium data (A simple circular Tokamak)

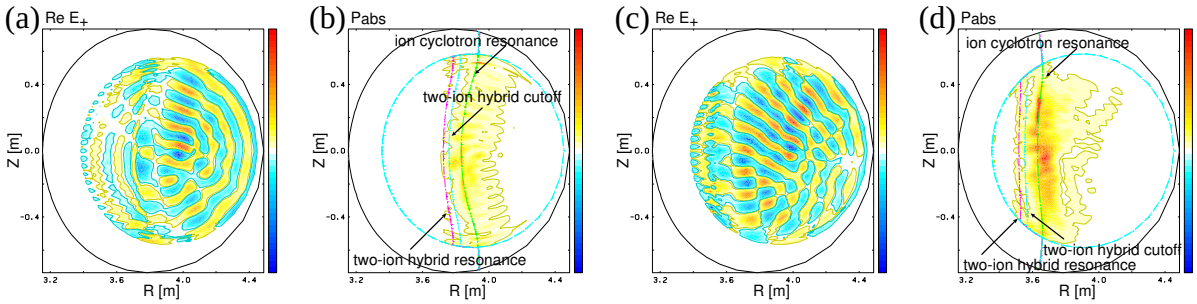

FIG. 3. Wave propagation and absorption in plasma by TASK/WM, (a) on axis heating case (f_{RF} = 42 MHz), (b) Off axis heating case (f_{RF} = 45 MHz)

Next, we analyzed the the evolution of velocity distribution function of minority ions and the plasma heating efficiency by GNET. The RF electric field profile obtained by TASK/WM is used to accelerate the minority ions following Eq. (6). The same plasma parameters are assumed as in the TASK/WM calculation. The test particle orbits are followed for about 0.6 s to obtain the steady state of the distribution function.

The velocity distribution function of minority ions are shown in Fig. 4 and 5. Fig. 4 are contour plots of the velocity distribution averaged on the flux surface between ρ ($= \sqrt{\psi/\psi_a}$) = 0.0 and 0.10 (left upper), ρ = 0.31 and 0.41 (right upper), and ρ = 0.45 and 0.55 (left lower), ρ = 0.66 and 0.76 (right lower) with f_{RF} = 42 MHz (on axis heating case). Fig. 5 shows those in the case of f_{RF} = 45 MHz (off axis heating case).

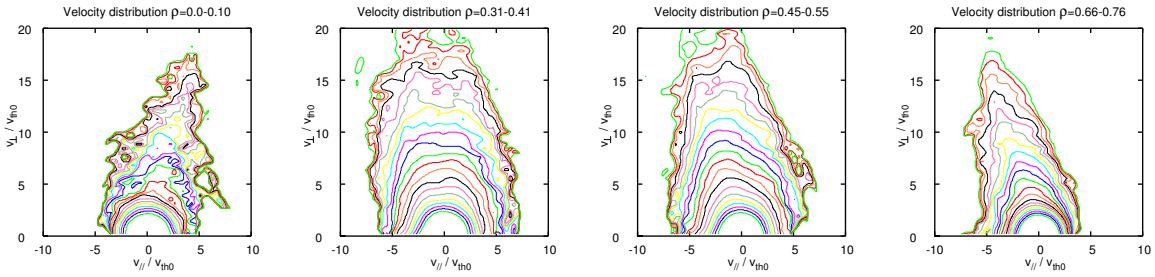

FIG. 4. Velocity distribution averaged in each radial interval, On axis heating case (f_{RF} = 42 MHz)

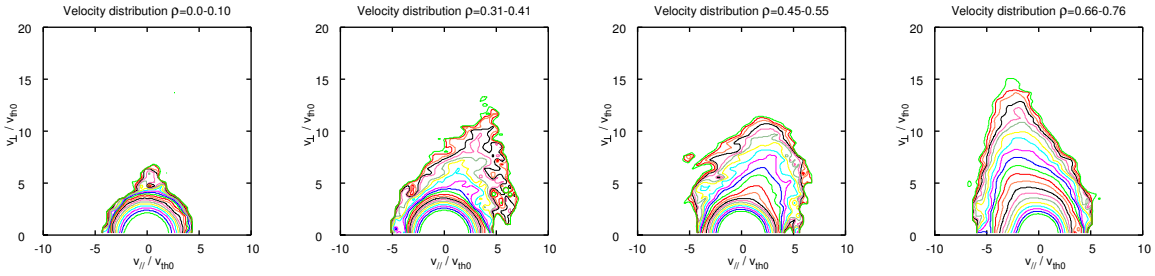

FIG. 5. Velocity distribution averaged in each radial interval, Off axis heating case (f_{RF} = 45 MHz)

In the on axis heating case, the perpendicular heating by ICRF waves near the magnetic axis is observed (Fig. 4 left), while, in the off axis heating case, the smaller perpendicular heating near the magnetic axis is observed than that of the on axis heating case.

In these velocity distribution, the asymmetry in the parallel velocity distribution can be seen. In Fig. 4, the minority ion distribution in the positive parallel velocity region is larger than that in the negative parallel velocity region between ρ = 0.0 and 0.10 (left upper). Then, such asymmetry disappears in the velocity distribution between ρ = 0.31 and 0.41 (right upper). While, in velocity distribution between ρ = 0.45 and 0.55 (left lower), and ρ = 0.67 and 0.74 (right lower), the minority ion distribution in the negative parallel velocity region is larger than that in the positive parallel velocity region. In Fig. 5, the similar asymmetry can be seen.

In order to clarify the mechanism generating these asymmetry structure in the velocity space we study the orbit of the energetic ions. Fig. 6 shows the velocity distribution near ρ = 0.71 (left) and the particle orbits in the Boozer coordinates setting the parallel and perpendicular velocity marked in the left figure (right). The starting point of the poloidal angle is assume to be 22 deg.

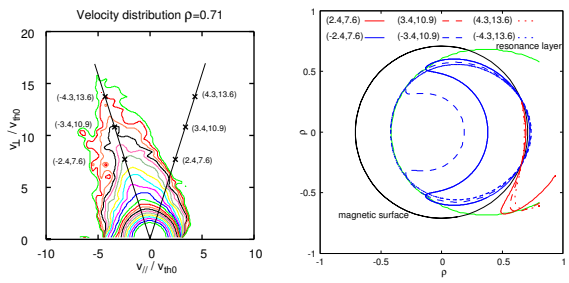

FIG. 6. Velocity distribution and particle orbit, On axis heating case (f_{RF} = 42 MHz)

It is found that the orbits show the trapped ones whose turning point are near the resonance layer. (The resonance layer becomes curved line in the Boozer coordinates.) Those particles

would stay long in the resonance region and be accelerated strongly. Therefore the velocity distribution in the specific pitch angle are increased.

Also we can see the finite orbit size effect in the left figure. It is observed that the particles with positive parallel velocity can be confine, while the particles with the negative parallel velocity are lost by the orbit loss, escaping from the plasma region. In this radial point, the distribution with the negative parallel velocity are larger than that with the positive parallel velocity. On the other hand, in the inner radial point, the particles with positive parallel velocity is large. The effect of finite orbit width results in the asymmetry with respect to parallel velocity distribution of energetic particles.

Figure 7 show the radial profile of the ICRF wave power absorbed by minority ions in the on axis heating case and off axis heating case, respectively. The left figure are results calculated by GNET and the right figure are those calculated by TASK/WM. The each radial peak positions of absorbed power calculated by GNET and TASK/WM are in good agreements. The heating efficiencies (Total heating power/Total power absorption) are 0.697 (On axis heating) and 0.396 (Off axis heating), respectively. This difference of efficiency is due to the large orbit loss in the off axis heating case.

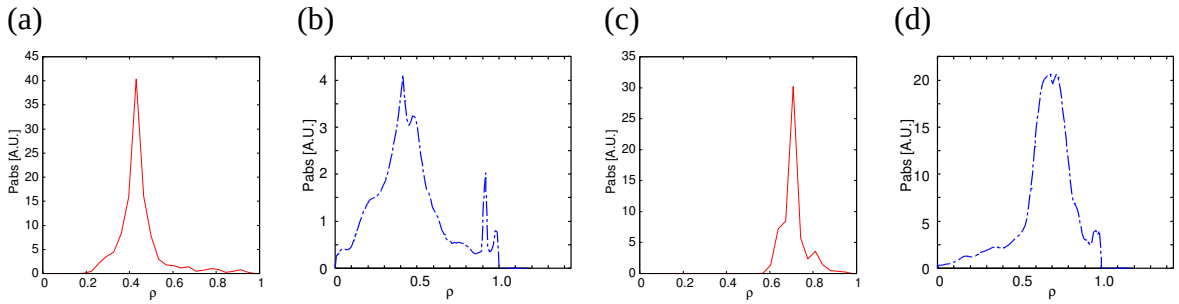

FIG. 7. Power absorption, (a) on axis heating case (f_{RF} = 42 MHz), (b) off axis heating case (f_{RF} = 45 MHz)

The asymmetry in the parallel velocity distribution generates the toroidal flow. We, finally, show the radial profile of toroidal velocity in Fig. 8. It is observed that the toroidal shear flow is generated by the ICRF heating because of the finite orbit width effect.

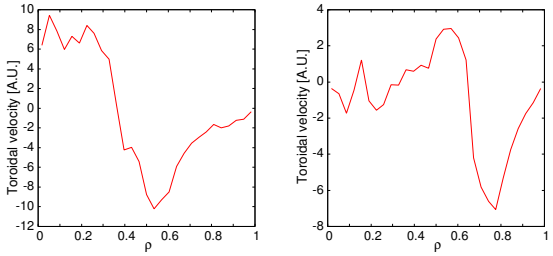

FIG. 8. Toroidal velocity, On axis heating case, f_{RF} = 42 MHz (left) and Off axis heating case, f_{RF} = 45 MHz (right)

5.3. Conclusion

We have been developing the global simulation code of ICRF heating combining the TASK/WM and GNET. We have carried out a global simulation of ICRF heating in a simple circular Toka-

mak. The realistic ICRF wave profile has been obtained by TASK/WM and has been used to solve a drift kinetic equation in the GNET.

We have found the asymmetry in the parallel velocity distribution and the asymmetry has depended on the radial position. Orbit analyses have indicated that the asymmetry arises from the finite orbit width effect of trapped particles and the asymmetry results in toroidal shear flow.

6. Advanced formulation of full wave analysis

In order to extend the integro-differential full wave analysis to more realistic situations, two approaches are newly formulated. One is to extend the integral formulation to arbitrary momentum distribution function rather than Maxwellian distribution. The other is to take account of the inhomogeneity of the magnetic field along the field line, which has been approximated by the toroidal dispersion function.

This work was supported in part by the Grant-in-Aid for Scientific Research, Nos. 19360451 and 20226017, from JSPS and the Grant-in-Aid for Specially Promoted Research, No. 16002005, from MEXT.

References

[1] FUKUYAMA, A., et al.: Proc. of 20th IAEA FEC (Villamoura, 2004) IAEA-CSP-25/CD/TH/P2-3.
[2] MURAKAMI, S., et al.: Nucl. Fusion **46** (2006) S425-S432.
[3] YAMAMOTO, T., MURAKAMI, S., FUKUYAMA, A., Plasma and Fusion Research **3** (2008) S1075.
[4] BOOZER, A.H., KUO-PETRAVIC, G., Phys. Fluids **24** (1981) 851.